

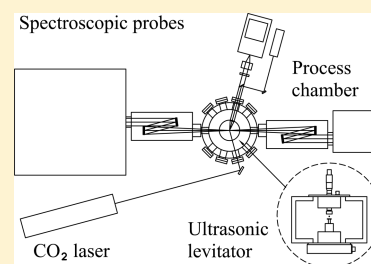
# In Situ Raman Spectroscopic Study of Gypsum ( $\text{CaSO}_4 \cdot 2\text{H}_2\text{O}$ ) and Epsomite ( $\text{MgSO}_4 \cdot 7\text{H}_2\text{O}$ ) Dehydration Utilizing an Ultrasonic Levitator

Stephen J. Brotton and Ralf I. Kaiser\*

Department of Chemistry and NASA Astrobiology Institute, University of Hawaii at Manoa, Honolulu, Hawaii 96822, United States

**ABSTRACT:** We present an original apparatus combining an acoustic levitator and a pressure-compatible process chamber. To characterize in situ the chemical and physical modifications of a levitated, single particle while heated to well-defined temperatures using a carbon dioxide laser, the chamber is interfaced to a Raman spectroscopic probe. As a proof-of-concept study, by gradually increasing the heating temperature, we observed the variations in the Raman spectra as 150  $\mu\text{g}$  of crystals of gypsum and epsomite were dehydrated in anhydrous nitrogen gas. We display spectra showing the decreasing intensities of the  $\nu_1$  symmetric and  $\nu_3$  asymmetric stretching modes of water with time and the simultaneous shift of the  $\nu_1(\text{SO}_4^{2-})$  symmetric stretch mode to higher wavenumbers. Our results demonstrate that the new apparatus is well suited to study the dehydration of levitated species such as minerals and offers potential advantages compared with previous experiments on bulk samples.

**SECTION:** Environmental and Atmospheric Chemistry, Aerosol Processes, Geochemistry, and Astrochemistry



Chemical reactions on the surfaces of micrometer- and nanometer-sized particles contribute significantly to the formation of astrochemically relevant molecules ranging from diatomic hydrogen ( $\text{H}_2$ ) to astrobiologically important complex species such as the sugar glycolaldehyde ( $\text{HCOCH}_2\text{OH}$ ) and even the amino acid glycine ( $\text{NH}_2\text{CH}_2\text{COOH}$ ).<sup>1</sup> Furthermore, surface reactions are relevant in the atmospheric sciences, as they have been implicated in, for example, the catalytic degradation of ozone in the terrestrial atmosphere<sup>2,3</sup> and in the redox chemistry of iron-oxide based grain particles in the martian atmosphere during dust storms.<sup>4</sup> Finally, the chemical growth of surfaces – possibly via resonantly stabilized free radicals (RSFRs), aromatic radicals (ARs), and polycyclic aromatic hydrocarbons (PAHs) – has been suggested to ultimately lead to carbonaceous grain particles (“soot”) during the incomplete combustion of fossil fuel, biofuel, and biomass.<sup>5–7</sup>

Thus far, most of our understanding of surface chemistry has been obtained from sophisticated surface-science techniques.<sup>8</sup> For example, a nonreactive or reactive species in the gas phase, which is often generated in an effusive or supersonic beam, interacts with a macroscopic surface at a well-defined temperature.<sup>9</sup> However, the study of physical and chemical processes on these “bulk” surfaces may differ from that on the surfaces of micrometer- or nanometer-sized particles<sup>10</sup> due to the large surface-to-volume ratio. Also, owing to the smaller heat capacity, the latent heat released by chemical reactions on the surfaces of micrometer-sized particles may lead to significant heating, whereas the transfer of reaction energy to a bulk surface usually produces negligible effects. Furthermore, for sufficiently small particles, the radius of curvature of the surface can affect the reactions.<sup>11</sup> Finally, the diffusion of radicals could be significant on isolated grains but may produce

only minor, localized effects on bulk samples.<sup>10</sup> As a well-known example, the chemistry of ozone depletion caused by photochemical reactions on the surfaces of the polar stratospheric cloud (PSC) particles differs significantly from the laboratory simulations using bulk ice surfaces.<sup>2,3,10</sup>

Several experimental techniques have been employed to trap and study micrometer- and nanometer-sized particles including Paul-traps using a low-frequency ( $\sim 100$  Hz) alternating electric field<sup>12</sup> and optical trapping by a laser beam.<sup>13</sup> For instance, the ignition and combustion of levitated aluminum particles has been studied by Marion et al.<sup>14</sup> using a carbon dioxide ( $\text{CO}_2$ ) laser combined with an electrodynamic levitator enclosed within a high-pressure chamber. Furthermore, Gerlich et al. employed high-resolution nanoparticle mass spectrometry to probe the surface of a single, isolated particle stored in a quadrupole trap and an infrared laser to control the temperature.<sup>11</sup> However, the electric and laser traps are sensitive to the physical properties of the samples such as the electric charge (Paul trap) and the refractive index (laser trap). Cloud chambers<sup>15</sup> have been used to investigate aerosols, but these experiments deal with the averages of the size, shape, and other properties of an ensemble of particles rather than an isolated, individual particle. Acoustic levitators have been employed by the analytical chemistry and material science communities in a diverse range of applications.<sup>16,17</sup> In an acoustic levitator, intense sound waves generated by a piezoelectric crystal reflect from a concave-shaped plate to generate a standing wave. The latter produces acoustic radiation pressure on the particle,<sup>18,19</sup> which counteracts the gravitational force. In

**Received:** November 15, 2012

**Accepted:** January 22, 2013

**Published:** January 22, 2013

accordance with Bernoulli's theorem, the maxima in the (time-averaged) kinetic energy density of the standing wave correspond to minima in the pressure.<sup>20</sup> Particles with diameters smaller than the wavelength of the sound are therefore levitated slightly below the pressure minima of the ultrasonic standing wave without the complicating effects of a contacting surface, which allows for so-called container-less processing. An advantage of acoustic levitation is versatility, that is any particle can be levitated independently of its refractive index or charge provided that a pressure between typically a few hundreds and a few thousands of Torr is maintained.

In this letter, we present a novel apparatus combining an acoustic levitator and a pressure-compatible process chamber. The chamber is interfaced to a Raman spectroscopic probe to characterize in situ and in real time any chemical and physical modifications of the levitated, single particle. In the present design, using a carbon dioxide laser, the levitated particles can be heated to well-defined temperatures up to  $\sim 600$  K. The chamber allows control of the gas temperature, pressure, and chemical composition to permit experiments related to astrochemistry, planetary chemistry, biochemistry, material sciences, atmospheric chemistry, and combustion processing.

To demonstrate the potential of the experimental setup, we studied the stepwise dehydration of levitated epsomite ( $\text{MgSO}_4 \cdot 7\text{H}_2\text{O}$ ) and gypsum ( $\text{CaSO}_4 \cdot 2\text{H}_2\text{O}$ ) crystals induced by heating from the carbon dioxide laser. These experiments have important implications for the understanding of our solar system. The OMEGA/Mars Express hyperspectral imager identified hydrated sulfates such as kieserite ( $\text{MgSO}_4 \cdot \text{H}_2\text{O}$ ), gypsum, and polyhydrated sulfates on the martian surface.<sup>21</sup> Furthermore, the Galileo mission to Jupiter suggests that magnesium sulfate in various stages of hydration is present on the surface of Europa<sup>22</sup> and Ganymede.<sup>23</sup> To understand the hydrologic history of Mars and some of Jupiter's and Saturn's moons, future missions need to identify in situ the hydration states of sulfates including magnesium sulfate ( $\text{MgSO}_4 \cdot n\text{H}_2\text{O}$ ;  $n = 7, 6, \dots, 0$ ),<sup>24</sup> gypsum, bassanite ( $\text{CaSO}_4 \cdot 0.5\text{H}_2\text{O}$ ), and anhydrite ( $\text{CaSO}_4$ ). Raman spectroscopy is ideally suited for this purpose because the Raman spectrum for each different degree of hydration is unique.

We first consider the stepwise dehydration of gypsum, which can transform into bassanite and anhydrite. A gypsum crystal with a mass of about  $150 \mu\text{g}$  was levitated in anhydrous nitrogen gas at atmospheric pressure. The grain was irradiated by the carbon dioxide laser at a 5% duty cycle, which corresponds to a power of 2 W and temperature of approximately 400 K (see the Experimental Methods). Figure 1 (top) shows the variation of the Raman spectrum in the high-shift region as water molecules are progressively removed from gypsum. The peak positions at approximately  $3412$  and  $3501 \text{ cm}^{-1}$  correspond to the  $\nu_1$  symmetric stretch and  $\nu_3$  asymmetric stretch modes of water, respectively. The disappearance of the water peaks in Figure 1 (top) demonstrates that the transition from gypsum to anhydrite is complete. The corresponding spectra in the low Raman-shift region are presented in Figure 1 (bottom). Before irradiation, gypsum produces peaks at  $1008$  and  $1136 \text{ cm}^{-1}$  due to the  $\nu_1$  symmetric stretch and  $\nu_3$  asymmetric stretch modes of the sulfate anion ( $\text{SO}_4^{2-}$ ), respectively. As the sample is progressively dehydrated, the peaks at  $1008$  and  $1136 \text{ cm}^{-1}$  reduce in amplitude, whereas a new peak appears at around  $1026 \text{ cm}^{-1}$ . The variation in the  $\nu_1(\text{SO}_4^{2-})$  mode shown in Figure 1 (bottom) is a consequence of removing water

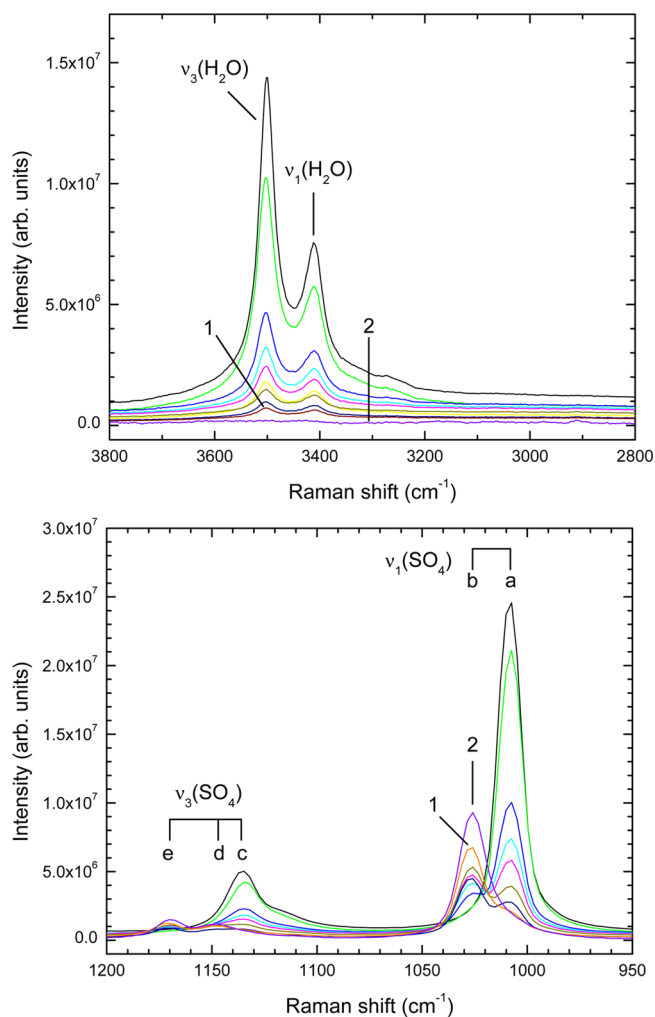


**Figure 1.** Variation of the Raman spectra in the low (bottom figure) and high (top figure) shift regions as a grain of gypsum ( $\text{CaSO}_4 \cdot 2\text{H}_2\text{O}$ ) levitated in anhydrous nitrogen is dehydrated to anhydrite ( $\text{CaSO}_4$ ) by irradiation from a carbon dioxide laser. The labels 1 and 2 refer to the specific irradiation times and temperatures described in the text. The wavenumbers of the peak maxima, including those labeled a–e, are presented in Table 1.

molecules, which affects the crystallographic environment and, hence, the distortion of the  $\text{SO}_4^{2-}$  tetrahedra.<sup>25</sup> Additional information regarding the changes in the crystal structure could be obtained by combining acoustic levitation with synchrotron X-ray diffraction (XRD) measurements.<sup>26</sup> The penultimate spectra (see curves (1)) in Figure 1 were obtained by irradiating gypsum with the carbon dioxide laser for 7 h 20 min at the power of 2 W. The small quantity of water remaining was subsequently removed by further irradiation for 80 min at 2.4 W or around 420 K (curves (2)). According to Sarma et al.,<sup>25</sup> for a relative humidity of about 60% the onset temperature for the formation of anhydrite is  $448 \pm 5$  K. The lower onset temperature for anhydrite production observed here might be expected due to levitation in anhydrous nitrogen.

We next discuss the dehydration of epsomite ( $\text{MgSO}_4 \cdot 7\text{H}_2\text{O}$ ), which can transform into  $\text{MgSO}_4 \cdot n\text{H}_2\text{O}$ , where  $n = 6, 5, \dots, 0$ . An epsomite crystal with a mass of about  $150 \mu\text{g}$  was levitated in anhydrous nitrogen gas at atmospheric pressure. The Raman spectra in the low-frequency shift range are shown in Figure 2 (bottom) as water molecules are progressively

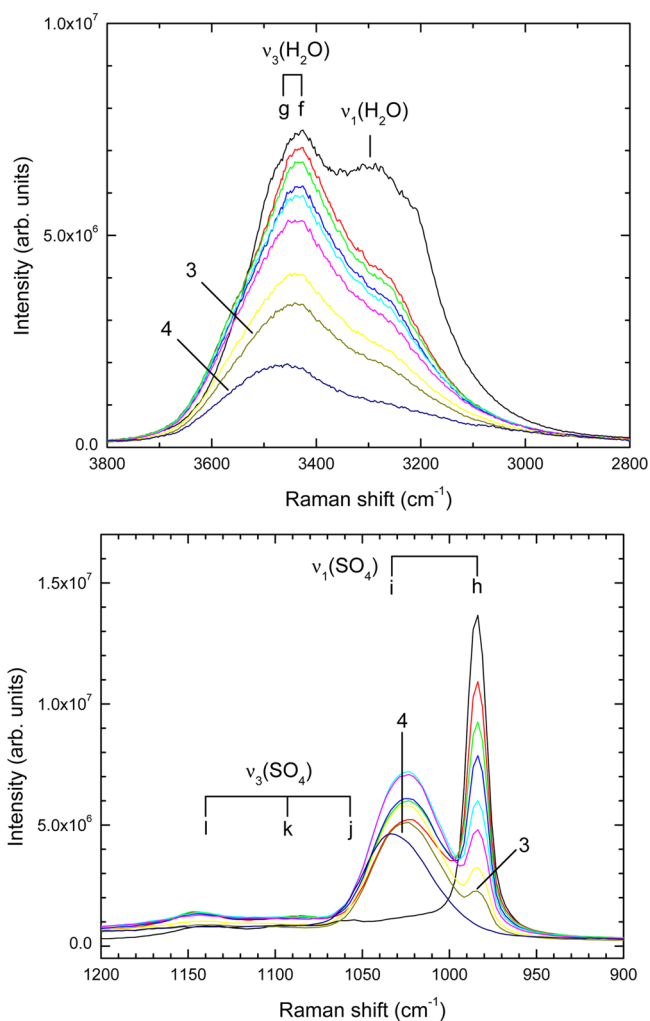


**Figure 2.** Variation of the Raman spectra in the low (bottom figure) and high (top figure) shift regions as a grain of epsomite ( $\text{MgSO}_4 \cdot 7\text{H}_2\text{O}$ ) levitated in anhydrous nitrogen dehydrates probably to sanderite ( $\text{MgSO}_4 \cdot 2\text{H}_2\text{O}$ ). The labels 3 and 4 refer to the specific irradiation times and temperatures described in the text. The wavenumbers of the peak maxima, including those labeled g–l, are presented in Table 1.

removed. Epsomite produces a large peak at  $984\text{ cm}^{-1}$  due to the  $\nu_1$  symmetric stretching mode of  $\text{SO}_4^{2-}$ . We first levitated the particle without irradiation from the carbon dioxide laser and, as a result of dehydration in the anhydrous nitrogen gas, the amplitude of the  $984\text{ cm}^{-1}$  peak reduced while a new peak appeared at about  $1023\text{ cm}^{-1}$ . The spectrum after 6 h (curve (3)) shows that a small peak at  $984\text{ cm}^{-1}$  remains, which suggests that the transformation to the new phase is not complete. Further significant changes to the spectra were not observed following levitation without heating for an extra 17 h 20 min. To remove additional water molecules, we therefore heated the particle by increasing the laser power from 1 to 2.4 W over a period of 7 h 20 min, which corresponds to a temperature range of approximately 350 to 420 K. The  $984\text{ cm}^{-1}$  peak was consequently observed to vanish, whereas the  $1023\text{ cm}^{-1}$  peak shifted to  $1033\text{ cm}^{-1}$  (curve (4)). The measurements of Wang et al.<sup>24</sup> show that the  $\nu_1(\text{SO}_4^{2-})$  peak in  $\text{MgSO}_4 \cdot 2\text{H}_2\text{O}$  (sanderite) and  $\text{MgSO}_4 \cdot 3\text{H}_2\text{O}$  occurs at  $1033.8$  and  $1023.8\text{ cm}^{-1}$ , respectively, and so the present spectra suggest that epsomite has dehydrated to sanderite with

$\text{MgSO}_4 \cdot 3\text{H}_2\text{O}$  as a possible intermediate phase. To show the corresponding variation of the water peaks, the high Raman-shift region is presented in Figure 2 (top). Before irradiation, the main water structure is composed of peaks at about  $3297$  and  $3428\text{ cm}^{-1}$  produced by the  $\nu_1$  symmetric stretch and  $\nu_3$  asymmetric stretch modes of water, respectively. There is also a suggestion of a weaker band at approximately  $3210\text{ cm}^{-1}$  arising from the first overtone of the  $\nu_2$  bending mode of water. Figure 2 (top) shows that upon dehydration the intensities of the water lines reduce significantly and, on average, move to higher Raman shifts with a maximum at  $3463\text{ cm}^{-1}$  (see Table 1). In

**Table 1.** Measured Wavenumbers  $\bar{\nu}$  of the Raman Bands for Gypsum, Anhydrite, Epsomite, and Sanderite<sup>†</sup>

| vibrational mode            | gypsum $\bar{\nu}$ ( $\text{cm}^{-1}$ ) | anhydrite $\bar{\nu}$ ( $\text{cm}^{-1}$ ) | epsomite $\bar{\nu}$ ( $\text{cm}^{-1}$ )          | sanderite $\bar{\nu}$ ( $\text{cm}^{-1}$ ) |
|-----------------------------|---|--|--|--|
| $\nu_1(\text{SO}_4^{2-})$   | $1008 \pm 1^a$                          | $1026 \pm 1^b$                             | $984 \pm 1^h$                                      | $1033 \pm 1^i$                             |
| $\nu_3(\text{SO}_4^{2-})$   | $1136 \pm 1^c$                          | $1147 \pm 1^d$<br>$1170 \pm 1^e$           | $1057 \pm 2^j$<br>$1093 \pm 3^k$<br>$1140 \pm 3^l$ |  |
| $\nu_1(\text{H}_2\text{O})$ | $3412 \pm 1$                            |  | $3297 \pm 6$                                       |  |
| $\nu_3(\text{H}_2\text{O})$ | $3501 \pm 1$                            |  | $3428 \pm 3^f$                                     | $3463 \pm 4^g$                             |

<sup>†</sup>Superscripts a–l correspond to the peak maxima labelled in Figures 1 and 2. The quoted errors combine the uncertainties from determining the band wavenumbers in the fitting procedure and calibrating the wavenumber scale using cyclohexane.

an attempt to further reduce the intensity of the water bands, the laser power was increased above 2.4 W. Consequently the background was found to increase rapidly, whereas the peaks became broader and reduced in amplitude. It was therefore not possible to obtain spectra with an acceptable statistical accuracy showing a significant further reduction in the intensity of the water lines relative to curve 4 in Figure 2 (top). The loss of sharp and detailed structure and the rising background are a consequence of the destruction of the crystal structure and the formation of an amorphous phase caused by the dehydration and heating.<sup>24</sup>

In conclusion, we have demonstrated that the new apparatus is well suited to observe the variations in the Raman spectra as gypsum and epsomite are dehydrated. The approach of levitating and heating particles with a carbon dioxide laser has advantages compared with previous experiments on bulk samples. First, the present apparatus offers the possibility of more precise control and measurement of the particle temperature. Owing to the small heat capacity, the levitated particles can be heated to high temperatures over very short time scales and be cooled more rapidly. Second, the small particle volume means that dehydration or rehydration processes occur more rapidly than for bulk samples. Third, as the levitator is enclosed within a process chamber, the environmental conditions such as the gas pressure and composition can be controlled and toxic chemicals contained. The relative humidity of the gas introduced into the process chamber could be varied using a humidity controller or by mixing anhydrous and water-saturated gas in different combinations.<sup>27</sup> By thus varying the humidity in the region of the levitated particle, it would be possible to investigate rehydration processes. Fourth, in an extension of the present work, the incorporation of a closed-cycle helium refrigerator or liquid nitrogen based cooling system will be used to reduce the temperature of the buffer gas in the process chamber to those

found on planets and their moons. The cooling system will help us explore the condensation of volatile gases of planetary relevance such as water and ammonia on mineral surfaces.<sup>10,28</sup> The new apparatus is well suited to investigating the dehydration of less-studied samples such as other minerals of planetary importance and biological samples. The experiments can also be extended to study combustion-relevant processes such as the growth of soot particles.

## EXPERIMENTAL METHODS

A schematic diagram of the experimental apparatus together with the levitator is presented in Figure 3. The Tec5 AG,

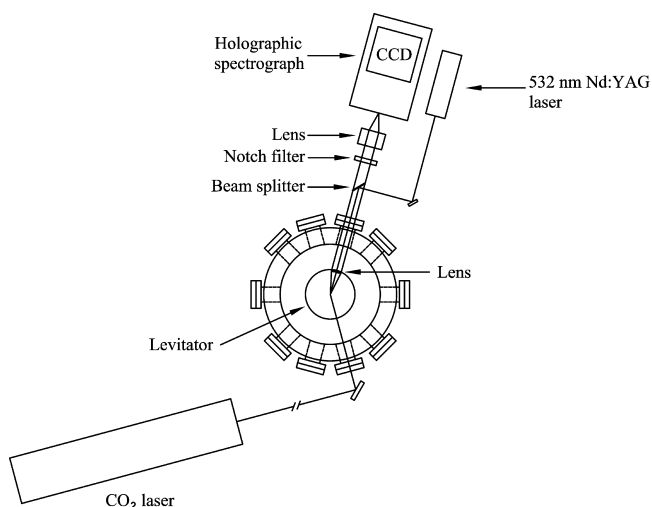


**Figure 3.** Schematic diagram of the levitator apparatus displaying the ultrasonic levitator, process chamber, carbon dioxide laser, and Raman spectrometer. For illustration purposes, the carbon dioxide laser is shown moved closer to the chamber. The multiple ports around the chamber are for the sample transfer manipulator, temperature sensor, and prospective analytical devices [Fourier transform infrared (FTIR) and UV–Vis spectrometers].

Sensorik und Systemtechnik acoustic levitator with modified supports is shown in more detail in Figure 4 within the process chamber. In brief, ultrasonic sound waves are generated by a piezoelectric transducer, which oscillates at 58 kHz producing a wavelength  $\lambda$  of about 5.9 mm in air at standard temperature and pressure. Owing to multiple reflections between the transducer and the concave reflector, a standing wave is generated. The distance between the front plate of the transducer and the reflector is usually set to  $2.5\lambda$  giving 5 pressure minima. A micrometer manipulator allows the distance between the transducer plate and reflector to be adjusted to an integral number of half wavelengths; therefore, the resonance conditions can be maintained following any changes in the gas composition, temperature, or pressure. Owing to acoustic radiation pressure, solid or liquid samples are levitated without contact slightly below the pressure minima. The largest diameter that can be levitated in the present levitator is approximately 2.5 mm, whereas the smallest is around 15  $\mu\text{m}$ . The levitator is enclosed within a process chamber, which permits pressures in the required range between a few hundred and a few thousand Torr. The experiments described in the present letter were performed at atmospheric pressure. The chamber allows levitation in an inert or anhydrous gas, such as nitrogen used in the present experiments. In contrast, one can

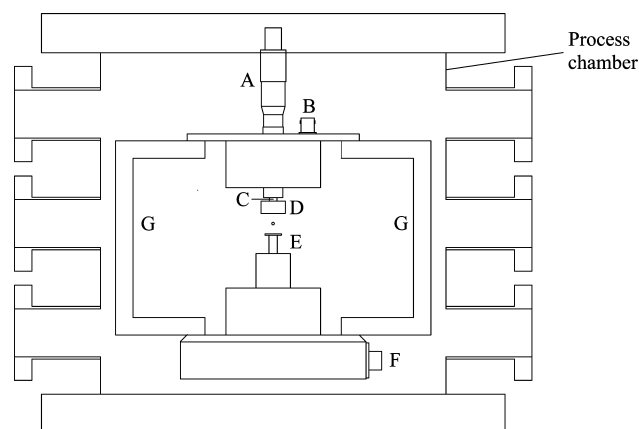


**Figure 4.** Schematic diagram of the levitator (A–G) and process chamber. Ultrasonic sound waves are generated by the piezoelectric transducer (E). Owing to multiple reflections between the transducer and the concave reflector (D), a standing wave is generated. A micrometer (A) allows the distance between the transducer plate and the reflector to be adjusted to an integral number of half wavelengths. The pressure amplitude of the standing wave is monitored by connecting the output of the piezoelectric sensor (C) via connector (B) to an oscilloscope. The RF power to the transducer is input via connector F, and G denotes a support.

introduce highly reactive gases to study reactions between the gas and the particle, possibly enhanced by heating from the carbon dioxide laser.

To heat the levitated particles, we used a 40 W carbon dioxide laser emitting at 10.6  $\mu\text{m}$  from Synrad. The output power of the laser can be adjusted between 1 and 40 W by varying the duty cycle of the discharge. A planar copper mirror and zinc selenide (ZnSe) windows on the chamber are used to transport the infrared beam to the levitated particle, which is located 104 cm from the exit of the laser as measured along the beam's path. The diameter of the beam exiting the laser is  $2.5 \pm 0.5$  mm and the beam divergence (full angle)  $< 7.0$  mR. Consequently, the diameter of the laser beam at the trap center is approximately 10 mm, which facilitates aligning the beam on the particle. When heated by the carbon dioxide laser, the particle spins rapidly around the central, vertical axis of the levitator. Therefore, although the irradiation is from one side of the chamber only, all surfaces of the particle are heated resulting in a more homogeneous sample temperature. The temperature of the levitated particles can be calculated using the requirement that, in thermal equilibrium, the radiation power absorbed from the carbon dioxide laser and surroundings must equal the power radiated by the particle plus the heat loss by conduction.<sup>29</sup> The heating of the air around the particle places an upper limit on the maximum temperature achievable for acoustically levitated particles.<sup>30</sup> In the future, we will determine the temperature of the particle via its blackbody spectrum.

A schematic diagram of the Raman spectrometer is included in Figure 3. The Raman transitions are excited by the 532 nm line of a frequency doubled, Q-switched Nd:YAG laser. The beam splitter reflects the laser beam incident at  $45^\circ$  toward the sample but transmits the longer Raman-shifted wavelengths of the backscattered photons. A lens with a focal length of 60 mm focuses the laser beam onto the sample and, by increasing the collection solid angle of the backscattered photons, significantly increases the count rate. In addition to the beam splitter, a 532

nm notch holographic filter prevents the intense 532 nm Rayleigh scattered beam from reaching and damaging the CCD camera. The Raman-shifted, backscattered photons are focused by a camera lens through a 100  $\mu\text{m}$  slit into a HoloSpec  $f/1.8$  holographic imaging spectrograph equipped with a thermoelectrically cooled, gated CCD camera from Princeton Instruments. The two overlaid holographic transmission gratings simultaneously cover the spectral ranges from 168–2388  $\text{cm}^{-1}$  and 2265–4387  $\text{cm}^{-1}$  with a resolution of 9  $\text{cm}^{-1}$ . Because we used a pulsed laser and CCD detector gated with an open period of 50 ns, no smearing of the spectra occurs if the particle spins rapidly.<sup>29</sup> The Raman shift scale was calibrated using cyclohexane and is estimated to be accurate to within 1  $\text{cm}^{-1}$ . Acoustic levitation has previously been combined with Raman spectroscopy<sup>31–33</sup> or a carbon dioxide laser<sup>34,35</sup> but, to our knowledge, not both simultaneously.

## AUTHOR INFORMATION

### Notes

The authors declare no competing financial interest.

## ACKNOWLEDGMENTS

This work was supported by the UH NASA Astrobiology Institute (R.I.K., S.J.B.).

## REFERENCES

- (1) Williams, D. A.; Herbst, E. It's a Dusty Universe: Surface Science in Space. *Surf. Sci.* **2002**, *500*, 823–837.
- (2) Solomon, S.; Garcia, R. R.; Rowland, F. S.; Wuebbles, D. J. On the Depletion of Antarctic Ozone. *Nature* **1986**, *321*, 755–758.
- (3) Tolbert, M. A.; Rossi, M. J.; Malhotra, R.; Golden, D. M. Reaction of Chlorine Nitrate with Hydrogen Chloride and Water at Antarctic Stratospheric Temperatures. *Science* **1987**, *238*, 1258–1260.
- (4) Bishop, J. L.; Murchie, S. L.; Pieters, C. M.; Zent, A. P. A Model for Formation of Dust, Soil, and Rock Coatings on Mars: Physical and Chemical Processes on the Martian Surface. *J. Geophys. Res.: Planets* **2002**, *107* (E11), 5097.
- (5) Richter, H.; Howard, J. B. Formation and Consumption of Single-Ring Aromatic Hydrocarbons and Their Precursors in Premixed Acetylene, Ethylene and Benzene Flames. *Phys. Chem. Chem. Phys.* **2002**, *4*, 2038–2055.
- (6) Richter, H.; Granata, S.; Green, W. H.; Howard, J. B. Detailed Modeling of PAH and Soot Formation in a Laminar Premixed Benzene/Oxygen/Argon Low-Pressure Flame. *Proc. Combust. Inst.* **2005**, *30*, 1397–1405.
- (7) Whitesides, R.; Kollias, A. C.; Domin, D.; Lester, W. A., Jr.; Frenklach, M. Graphene Layer Growth: Collision of Migrating Five-Member Rings. *Proc. Combust. Inst.* **2007**, *31*, 539–546.
- (8) Woodruff, D. P.; Delchar, T. A. *Modern Techniques of Surface Science*; Cambridge University Press: Cambridge, U.K., 1994.
- (9) Arumainayagam, C. R.; Madix, R. J. Molecular Beam Studies of Gas-Surface Collision Dynamics. *Prog. Surf. Sci.* **1991**, *38*, 1–102.
- (10) Mason, N. J.; Drage, E. A.; Webb, S. M.; Dawes, A.; McPheat, R.; Hayes, G. The Spectroscopy and Chemical Dynamics of Microparticles Explored Using an Ultrasonic Trap. *Faraday Discuss.* **2008**, *137*, 367–376.
- (11) Schlemmer, S.; Wellert, S.; Windisch, F.; Grimm, M.; Barth, S.; Gerlich, D. Interaction of Electrons and Molecules with a Single Trapped Nanoparticle. *Appl. Phys. A: Mater. Sci. Process.* **2004**, *78*, 629–636.
- (12) Gerlich, D. Molecular Ions and Nanoparticles in RF and AC Traps. *Hyperfine Interact.* **2003**, *146/147*, 293–306.
- (13) Neuman, K. C.; Block, S. M. Optical Trapping. *Rev. Sci. Instrum.* **2004**, *75*, 2787–2809.
- (14) Marion, M.; Chauveau, C.; Gökalp, I. Studies on the Ignition and Burning of Levitated Aluminum Particles. *Combust. Sci. Technol.* **1996**, *115*, 369–390.
- (15) Li, S.; Silvers, S. J.; ElShall, M. S. Surface Oxidation and Luminescence Properties of Weblike Agglomeration of Silicon Nanocrystals Produced by a Laser Vaporization-Controlled Condensation Technique. *J. Phys. Chem. B.* **1997**, *101*, 1794–1802.
- (16) Trinh, E. H. Compact Acoustic Levitation Device for Studies in Fluid Dynamics and Material Science in the Laboratory and Microgravity. *Rev. Sci. Instrum.* **1985**, *56*, 2059–2065.
- (17) Santesson, S.; Nilsson, S. Airborne Chemistry: Acoustic Levitation in Chemical Analysis. *Anal. Bioanal. Chem.* **2004**, *378*, 1704–1709.
- (18) Wang, T. G.; Lee, C. P. *Nonlinear Acoustics*; Hamilton, M. F., Blackstock, D. T., Eds.; Academic Press: San Diego, CA, 1998; Ch. 6.
- (19) Xie, W. J.; Wei, B. Parametric Study of Single-Axis Acoustic Levitation. *Appl. Phys. Lett.* **2001**, *79*, 881–883.
- (20) Brandt, E. H. Acoustic Physics - Suspended by Sound. *Nature* **2001**, *413*, 474–475.
- (21) Gendrin, A.; et al. Sulfates in Martian Layered Terrains: the OMEGA/Mars Express View. *Science* **2005**, *307*, 1587–1591.
- (22) McCord, T. B.; et al. Salts on Europa's Surface Detected by Galileo's Near Infrared Mapping Spectrometer. *Science* **1998**, *280*, 1242–1245.
- (23) McCord, T. B.; Hansen, G. B.; Hibbitts, C. A. Hydrated Salt Minerals on Ganymede's Surface: Evidence of an Ocean Below. *Science* **2001**, *292*, 1523–1525.
- (24) Wang, A.; Freeman, J. J.; Jolliff, B. L.; Chou, I. M. Sulfates on Mars: A Systematic Raman Spectroscopic Study of Hydration States of Magnesium Sulfates. *Geochim. Cosmochim. Acta* **2006**, *70*, 6118–6135.
- (25) Sarma, L. P.; Prasad, P. S. R.; Ravikumar, N. Raman Spectroscopic Study of Phase Transitions in Natural Gypsum. *J. Raman Spectrosc.* **1998**, *29*, 851–856.
- (26) Cerenius, Y.; Oskarsson, A.; Santesson, S.; Nilsson, S.; Kloo, L. Preliminary Tests on the Use of an Acoustic Levitator for Liquid X-ray Diffraction Experiments. *J. Appl. Cryst.* **2003**, *36*, 163–164.
- (27) Schlegel, M. C.; Wenzel, K.-J.; Sarfraz, A.; Panne, U.; Emmerling, F. A Wall-Free Climate Unit for Acoustic Levitators. *Rev. Sci. Instrum.* **2012**, *83*, 055101.
- (28) Bauerecker, S.; Neidhart, B. Formation and Growth of Ice Particles in Stationary Ultrasonic Fields. *J. Chem. Phys.* **1998**, *109*, 3709–3712.
- (29) Brotton, S. J.; Kaiser, R. I. *Rev. Sci. Instrum.* **2013**, in preparation.
- (30) Lee, C. P.; Wang, T. G. Acoustic Radiation Force on a Heated Sphere Including the Effects of Heat Transfer and Acoustic Streaming. *J. Acoust. Soc. Am.* **1988**, *83*, 1324–1331.
- (31) Leopold, N.; Haberkorn, M.; Laurell, T.; Nilsson, J.; Baena, J. R.; Frank, J.; Lendl, B. On-Line Monitoring of Airborne Chemistry in Levitated Nanodroplets: In Situ Synthesis and Application of SERS-Active Ag-Sols for Trace Analysis by FT-Raman Spectroscopy. *Anal. Chem.* **2003**, *75*, 2166–2171.
- (32) Santesson, S.; Johansson, J.; Taylor, L. S.; Levander, I.; Fox, S.; Sepaniak, M.; Nilsson, S. Airborne Chemistry Coupled to Raman Spectroscopy. *Anal. Chem.* **2003**, *75*, 2177–2180.
- (33) Schenk, J.; Trobs, L.; Emmerling, F.; Kneipp, J.; Panne, U.; Albrecht, M. Simultaneous UV/Vis Spectroscopy and Surface Enhanced Raman Scattering of Nanoparticle Formation and Aggregation in Levitated Droplets. *Anal. Methods* **2012**, *4*, 1252–1258.
- (34) Ermoline, A.; Schoenitz, M.; Hoffmann, V. K.; Dreizin, E. L. Experimental Technique for Studying High-Temperature Phases in Reactive Molten Metal Based Systems. *Rev. Sci. Instrum.* **2004**, *75*, 5177–5185.
- (35) Weber, J. K. R.; Hampton, D. S.; Merkley, D. R.; Rey, C. A.; Zatarski, M. M.; Nordine, P. C. Aero-acoustic Levitation - a Method for Containerless Liquid-Phase Processing at High Temperatures. *Rev. Sci. Instrum.* **1994**, *65*, 456–465.